Laser Optical Feedback Imaging (LOFI) controlled by an electronic feedback loop.

Pierre Guillemé, Eric Lacot, Olivier Jacquin, Wilfried Glastre, Olivier Hugon, Hugues Guillet de Chatellus

Laser Optical Feedback Imaging (LOFI) controlled by an electronic feedback loop.

Pierre Guillemé, Eric Lacot,* Olivier Jacquin, Wilfried Glastre, Olivier Hugon and Hugues Guillet de Chatellus

Centre National de la Recherche Scientifique/ Université de Grenoble 1, Laboratoire Interdisciplinaire de Physique, UMR 5588, Grenoble F- 38402, France

**Corresponding author: eric.lacot@ujf-grenoble.fr*

In autodyne interferometry, the beating between the reference beam and the signal beam takes place inside the laser cavity and therefore the laser fulfills simultaneously the roles of emitter and detector of photons. In these conditions, the laser relaxation oscillations play a leading role, both in the laser quantum noise which determines the signal to noise ratio (SNR) and also in the laser dynamics which determines the response time of the interferometer. In the present study, we have experimentally analyzed the SNR and the response time of a Laser Optical Feedback Imaging (LOFI) interferometer based on a Nd^{3+} microchip laser, with a relaxation frequency in the megahertz range. More precisely, we have compared the image quality obtained, when the laser dynamics is free and when it is controlled by a stabilizing electronic feedback loop using a differentiator. From this study, we can conclude that when the laser time response is shorter (i.e. the LOFI gain is lower), the image quality can be better (i.e. the LOFI SNR can be higher) and that the use of an adapted electronic feedback loop allows high speed LOFI with a shot-noise limited

sensitivity. Despite the critical stability of the electronic feedback loop, the obtained experimental results are in good agreement with the theoretical predictions.

OCIS codes: 110.3175, 280.3420.

1. INTRODUCTION

When a frequency shift is introduced between the two beams of an interferometer, one realizes the so-called heterodyne interferometry. Resulting from this shift, the interference between the two waves produces an intensity modulation at the beat frequency, which can be measured by a photo-detector. In this paper, we refer only to autodyne laser interferometry where the heterodyne wave mixing takes place inside the cavity of the laser source and is finally indirectly detected by a photodiode.

Since the development of the first laser in 1960, laser heterodyne interferometry has become a useful technique on which many high accuracy measurement systems for scientific and industrial applications are based [1]. Since the pioneer work of K. Otsuka, on self-mixing modulation effects in class-B laser [2] the sensitivity of laser dynamics to frequency-shifted optical feedback has been used in autodyne interferometry and metrology [3], for example in self-mixing laser Doppler velocimetry [4-7], vibrometry [8-10], near field microscopy [11,12] and laser optical feedback imaging (LOFI) experiments [13-16]. Compared to conventional optical heterodyne detection, frequency-shifted optical feedback shows an intensity modulation contrast higher by several orders of magnitude and the maximum of the modulation is obtained when the shift frequency is resonant with the laser relaxation oscillation frequency [17]. In this condition, an optical feedback level as low as -170 dB (i.e. 10^{17} times weaker than the intracavity power) has been detected [5].

In previous papers [17-19], we have demonstrated that in autodyne interferometry, the main advantage of the resonant LOFI gain (defined by the ratio between the cavity damping rate and the population-inversion damping rate of the laser) is to raise the laser quantum noise over the detector noise in a relatively large frequency range around the laser relaxation frequency.

We have also established that to maximize the dynamical range of a LOFI setup, the best value of the shift frequency is not the relaxation frequency, but the frequency at which the amplified laser quantum noise is equal to the detection noise level [18,19]. Recently [20], through a whole analytical and numerical study, we have demonstrated that for a fixed integration time T_{int} of the detection, the best LOFI images (images with the best SNR) are always obtained when using the laser with the shortest laser time response τ_R, (i.e. the lowest LOFI gain) and that the detection is shot noise limited if the condition $T_{int} >> \tau_R$ is satisfied.

The main objective of this paper is to confirm experimentally theses theoretical predictions and to determine the best conditions to obtain images with the best SNR (i.e. shot-noise limited) as fast as possible. To do this, we have compared the images quality obtained with a Nd microchip laser when its temporal dynamics is free (corresponding to a long laser time response τ_R) and when it is controlled by a stable electronic feedback loop using a differentiator (giving a shorter laser time response $\tilde{\tau}_R < \tau_R$). Experimentally, the use of a differentiator circuit allows comparing two lasers (i.e. the free running laser and the controlled laser) with the same output power and the same relaxation frequency, but having two different values of the laser response time and therefore two different values of the LOFI gain.

This paper is organized as follows. Firstly, after a basic description of our LOFI setup with an electronic feedback loop, we briefly recall the LOFI SNR for different values of the experimental acquisition time (T_{int}) compared to the laser dynamical response time (τ_R). Secondly, the open loop transfer function of the electronic feedback is experimentally characterized and the stability of the closed loop is experimentally verified. Finally we determine the equivalent laser time response induced by the electronic differentiator. Thirdly, the LOFI SNRs experimentally

obtained with the free running laser and with the electronically controlled laser are compared. We finally determine the best experimental condition for high speed LOFI imaging.

2. LOFI WITH AN ELECTRONIC FEEDBACK LOOP

A. LOFI setup

A schematic diagram of the LOFI experimental setup (i.e. the autodyne experimental interferometer) is shown in Fig. 1. Typically the laser is an optically pumped CW microchip laser with an output power P_{out} of several milliwatts and a typical relaxation oscillation frequency F_R in the megahertz range and a damping rate of the relaxation oscillation ($1/\tau_R$) in the kilohertz range [19, 21]. The laser is therefore a class-B laser ($F_R >> 1/\tau_R$). The microchip laser beam is sent on the target, through a frequency shifter. A part of the light diffracted and/or scattered by the target is then reinjected inside the laser cavity after a second pass through the frequency shifter. Therefore, the optical frequency of the reinjected light is shifted by $F_e = \Omega_e/2\pi$. This frequency can be adjusted and is typically of the order of the laser relaxation frequency $F_R = \Omega_R/2\pi$. The laser beam waist and the laser focal spot on the target under investigation are optically conjugated. At this point, one can already notice that, compared to a conventional heterodyne setup, the autodyne setup shown here does not require complex alignment. Indeed, the LOFI setup is even always self-aligned because the laser simultaneously fulfills the function of the source (i.e. photons-emitter) and of the photo-detector (i.e. photons-receptor).

The optical feedback is characterized by the electric field complex reflectivity ($r_e = \sqrt{R_e}\exp(j\phi_e)$) of the target, where the phase ϕ_e describes the optical round trip between the laser and the target, while the effective power reflectivity ($R_e = |r_e|^2$) takes into account the target albedo, the numerical aperture of the collection optics, the frequency shifters efficiencies and the transmission of all optical components (except for the beam splitter which is addressed separately) and the overlap of the retro-diffused field with the Gaussian cavity beam (confocal feature).

The coherent interaction (beating) between the lasing electric field and the frequency-shifted reinjected field leads to a modulation of the laser output power at F_e. For the detection purpose, a fraction of the output beam of the microchip laser is sent to a photodiode by means of a beam splitter characterized by a power reflectivity R_{bs}. The photodiode is assumed to have a quantum efficiency of 100%. The voltage delivered by the photodiode is finally analyzed by a lock-in amplifier which gives the LOFI signal (i.e. the magnitude and the phase of the retro-diffused electric field) at the demodulation frequency F_e [15,16]. The lock-in amplifier is characterized by its integration time T_{int}. Experimentally, the LOFI images are obtained pixel by pixel (i.e. point by point, line after line) by a full 2D galvanometric scanning and the necessary time needed to obtain an image composed of N pixels is roughly given by: $N \times T_{int}$. For high speed imaging (i.e. high cadence imaging), one needs to use a value of T_{int} as small as possible. To determine the SNR of the obtained LOFI images, T_{int} needs to be compared with the response time of the class-B laser (i.e. τ_R).In this paper, whatever the temporal values of T_{int} (in the

millisecond or microsecond range), we refer to a fast response time laser when: $\tau_R << T_{\text{int}}$ and to a slow response time laser when: $\tau_R >> T_{\text{int}}$.

In the present study, the laser dynamics (and more particularly the laser time response) can be controlled by an electronic feedback loop using a differentiator and acting on the pumping power by the way of an AOM (Acousto-Optic Modulator). More precisely, the AOM is supplied by a RF voltage which is proportional to the temporal derivative of the laser outpout power fluctuation. With this electronic control, the pumping power decreases (respectively increases) when the laser power increases (respectively decreases) which stabilize the laser power fluctuations. Experimentally, the use of an electronic differentiator allows the comparison of two kinds of laser dynamics. The free running laser, when the feedback loop is off (i.e. inactive), and the dynamically controlled laser, when the feedback loop is on (i.e. active). Due to the use of a differentiator, the two studied lasers have the same average output power and the same relaxation frequency, but have two different values of the laser response time and therefore two different values of the LOFI gain.

B. LOFI Modeling

In the case of weak ($R_e << 1$) frequency shifted optical feedback, the dynamical behavior of a re-injected solid-state laser can be described by the following set of equations [10, 17,18]:

$$\frac{dN}{dt} = \gamma_1 N_0 + \gamma_1 \Delta N_0(t) - \gamma_1 N - B N I + F_N(t), \tag{1a}$$

$$\frac{dI}{dt} = (BN - \gamma_c) I + 2\gamma_c \sqrt{R_e}(1 - R_{bs}) I \cos[2\pi F_e t + \phi_e] + F_I(t), \tag{1b}$$

where, N is the population inversion, I is the intra-cavity laser intensity (photon unit), B is related to the Einstein coefficient, γ_1 is the decay rate of the population inversion, γ_c is the laser cavity decay rate, $\gamma_1 N_0$ is the pumping rate and $\gamma_1 \Delta N_0(t)$ describes the pumping rate modification induced by the electronic feedback loop. Regarding the noise, the laser quantum fluctuations are described by the Langevin noise functions $F_N(t)$ and $F_I(t)$, which have a zero mean value and a white noise type correlation function [22-24]. In the set of Eqs. (1), the cosine function expresses the beating (i.e. the coherent interaction) between the lasing and the optical feedback electric field.

The laser model presented here can be applied to three levels or four levels lasers with the condition that the lifetime of the upper level of the pumping transition is very short compared to the lifetime of the upper level of the laser transition. For example, this is condition is satisfied in a three levels laser such as erbium lasers as well as for a four levels laser such as neodymium laser. In the LOFI modeling presented here, the feedback time delay (τ), linked to the optical round trip between the laser and the target is completely neglected. It means, that we only consider the case where the round trip time is much shorter than the inverse of the frequency shift ($2\pi F_e \tau << 1$).

To investigate the small fluctuations of the laser intensity and of the population inversion, Eqs.(1) are linearized around the steady state given by:

$$N_s = \frac{\gamma_c}{B} \tag{2a}$$

$$I_s = \frac{\gamma_1}{B}(A-1), \tag{2b}$$

where $A = \frac{N_0}{N_S}$ is the normalized pumping parameter. Using Eq. (2b) the average photon output rate of the laser (number of photons per second) is defined by: $p_{out} = \gamma_c I_s$. After the linearization of Eqs. (1), we take their Fourier Transforms, which converts the differential equations into algebraic equations. One obtains:

$$i\Omega\,\Delta N(\Omega) = -\gamma_1 A \Delta N(\Omega) + \gamma_1 \Delta N_0(\Omega) - \gamma_c \Delta I(\Omega) + F_N(\Omega) \tag{3a}$$

$$i\Omega\,\Delta I(\Omega) = B I_S \Delta N(\Omega) + 2\gamma_c \sqrt{R_e}(1 - R_{bs}) I_S \exp(i\phi_e)\frac{\delta(\Omega - \Omega_e)}{2} + F_I(\Omega) \tag{3b}$$

The use of the algebraic Eqs. (3), allows to determine the laser fluctuations $\Delta I(\Omega)$. Let us call $\Delta I_{LOFI}(\Omega)$: the laser fluctuations induced by the optical feedback (R_e), $\Delta I_{noise}(\Omega)$: the laser fluctuations induced by the laser quantum noise ($F_I(\Omega)$ and $F_N(\Omega)$) and $\Delta I_{pump}(\Omega)$: the laser fluctuations induced by the pump fluctuations ($\Delta N_0(\Omega)$).) One finally easily obtains:

$$\Delta I(\Omega) = \Delta I_{LOFI}(\Omega) + \Delta I_{noise}(\Omega) + \Delta I_{pump}(\Omega) \tag{4a}$$

with:

$$\Delta I_{LOFI}(\Omega) = G_{LOFI}(\Omega)\sqrt{R_e}(1 - R_{bs}) I_S\, \delta(\Omega - \Omega_e)\exp(i\phi_e) \tag{4b}$$

$$\Delta I_{pump}(\Omega) = G_{pump}(\Omega)\Delta N_0(\Omega) \tag{4c}$$

$$\Delta I_{noise}(\Omega) = G_{LOFI}(\Omega)\gamma_c^{-1} F_I(\Omega) + G_{pump}(\Omega)\gamma_1^{-1} F_N(\Omega) \tag{4d}$$

where the complex LOFI gain and the complex pumping gain are respectively given by :

$$G_{LOFI}(\Omega) = \frac{\gamma_c(i\Omega + \gamma_1 A)}{\Omega_R^2 - \Omega^2 + i\Omega\gamma_1 A} \tag{5}$$

$$G_{pump}(\Omega) = \frac{\gamma_1 B I_S}{\Omega_R^2 - \Omega^2 + i\Omega\gamma_1 A} = \frac{\gamma_1}{\gamma_c}\frac{\Omega_R^2}{\Omega_R^2 - \Omega^2 + i\Omega\gamma_1 A}, \tag{6}$$

where $\Omega_R^2 = \gamma_c B I_S = \gamma_1\gamma_c(A-1)$ is linked to the laser relaxation frequency $F_R = \Omega_R/2\pi$.

C. The Electronic Feedback Loop (EFL)

Due to the electronic feedback loop, the pump fluctuations $\Delta N_0(\Omega)$ and the laser fluctuations $\Delta I(\Omega)$ are linked through the following equation:

$$\Delta N_0(\Omega) = -g R_{bs} G_{AOM}(\Omega) G_{EFL}(\Omega) \Delta I(\Omega) \tag{7}$$

where $G_{AOM}(\Omega)$ is the transfer function of the AOM which control the pumping power, $G_{EFL}(\Omega)$ is the transfer function of the electronic differentiator and g is a proportionality constant which allows to convert the fluctuations of photons $[\Delta I(\Omega)]$ to the fluctuations of atoms $[\Delta N_0(\Omega)]$. At this point, one can also notice that a minus sign is applied in Eq. (7) in order that the feedback loop allows to decrease the fluctuations of the laser intensity [25]. Indeed, by combining Eqs. (4) and (7), one obtains:

$$\Delta I(\Omega, g) = \frac{\Delta I_{LOFI}(\Omega) + \Delta I_{noise}(\Omega)}{1 + G_{ofl}(\Omega, g)}, \tag{8}$$

where the gain of the open feedback loop is given by [26]:

$$G_{ofl}(\Omega, g) = gR_{bs}G_{AOM}(\Omega)G_{EFL}(\Omega)G_{pump}(\Omega). \quad (9)$$

At this point, one can notice that $g = 0$ (i.e. $G_{ofl}(\Omega,0) = 0$) allows to describe the conventional LOFI setup using a free running laser, while $g \neq 0$ (i.e. $G_{ofl}(\Omega, g) \neq 0$) allows to describe a LOFI imager controlled (i.e. stabilized) by the electronic feedback loop.

By using the photons output rate instead of the number of photons: $\Delta p_{out}(\Omega, g) = \gamma_c \Delta I(\Omega, g)$, the RF power spectrum $PS_{out}(\Omega, g)$ of the laser output power in presence of electronic feedback loop can be easily calculated using the usual definition of the spectral density function [17, 22, 23]:

$$2\pi PS_{out}(\Omega, g)\delta(\Omega + \Omega') = \langle \Delta p_{out}(\Omega, g)\Delta p_{out}(-\Omega', g) \rangle \quad (10)$$

Straightforward calculations give [27]:

$$PS_{out}(\Omega, g) = \frac{PS_{LOFI}(\Omega) + PS_{noise}(\Omega)}{|1 + G_{ofl}(\Omega, g)|^2} \quad (11a)$$

with for a strong class–B laser ($\Omega_R >> \gamma_1 A$) [17,18]:

$$PS_{LOFI}(\Omega) = R_e(1 - R_{bs})^2 p_{out}^2 |G_{LOFI}(\Omega)|^2 \delta(\Omega - \Omega_e) \quad (11b)$$

$$PS_{noise}(\Omega) \approx 2p_{out}|G_{LOFI}(\Omega)|^2, \quad (11c)$$

and therefore:

$$PS_{out}(\Omega,g) \approx \frac{|G_{LOFI}(\Omega)|^2}{|1+G_{ofl}(\Omega,g)|^2}\left[R_e p_{out}^2\,\delta(\Omega-\Omega_e)+2p_{out}\right]. \tag{12}$$

To make physics interpretation of this result, let us look at the ideal situation, where in the open loop gain $G_{ofl}(\Omega,g)$ defined by Eq. (9), the transfer function of the AOM controlling the pumping power is a pure normalized real function (i.e. a pure amplitude function introducing no phase shift):

$$G_{AOM}(\Omega)=1 \tag{13}$$

and where the electronic feedback loop uses a perfect RC differentiator, i.e. a high pass filter working far below the cut-off frequency Ω_c:

$$G_{EFL}(\Omega)=\frac{i\Omega}{\Omega_c+i\Omega}\underset{\Omega<<\Omega_c}{\approx} i\frac{\Omega}{\Omega_c} \tag{14}$$

By combining Eqs. (5) (6), (9) (13) and (14), one obtains easily, the square modulus of the equivalent LOFI gain:

$$\left|\tilde{G}_{LOFI}(\Omega,g)\right|^2=\frac{|G_{LOFI}(\Omega)|^2}{|1+G_{ofl}(\Omega,g)|^2}\underset{\Omega<<\Omega_c}{\approx}\frac{\gamma_c^2\left[\Omega^2+(\gamma_1 A)^2\right]}{\left(\Omega_R^2-\Omega^2\right)^2+\Omega^2\left[\gamma_1 A+gR_{bs}\frac{\gamma_1}{\gamma_c}\frac{\Omega_R^2}{\Omega_c}\right]^2} \tag{15}$$

Without the electronic feedback loop (i.e. $g=0$), one obtains:

$$\left|\tilde{G}_{LOFI}(\Omega,0)\right|^2=|G_{LOFI}(\Omega)|^2=\frac{\gamma_c^2\left[\Omega^2+(\gamma_1 A)^2\right]}{\left(\Omega^2-\Omega_R^2\right)^2+\Omega^2(\gamma_1 A)^2}\underset{\Omega_R>>\gamma_1 A}{\approx}\frac{\gamma_c^2}{4(\Omega-\Omega_R)^2+(\gamma_1 A)^2}, \tag{16}$$

which corresponds the conventional LOFI Lorentzian gain profile with a resonance width given by $\Delta\Omega_R = \gamma_1 A$, corresponding to a laser response time [20]:

$$\tau_R = \left(\frac{\gamma_1 A}{2}\right)^{-1} \tag{17}.$$

With the electronic feedback loop (i.e. $g > 0$), Eq. (15) shows that the resonance width is larger: $\Delta\widetilde{\Omega}_R(g) = \gamma_1 A + gR_{bs}\frac{\gamma_1}{\gamma_c}\frac{\Omega_R^2}{\Omega_c}$ and therefore the laser response time is shorter:

$$\widetilde{\tau}_R(g) = \left(\frac{\gamma_1 A + gR_{bs}\frac{\gamma_1}{\gamma_c}\frac{\Omega_R^2}{\Omega_c}}{2}\right)^{-1} \tag{18}$$

Finally, we conclude this section by reminding that the electronic feedback loop using a differentiator allows controlling the laser response time without any modification of the laser relaxation oscillations frequency and of the average value of laser output power.

D. LOFI SNR with the electronic feedback loop

Using a lock-in amplifier with an integration time T_{int}, the LOFI signal $\left(\widetilde{S}_{LOFI}(F_e, R_e, g)\right)$ and the LOFI noise $\left(\widetilde{N}_{LOFI}(F_e, T_{int}, g)\right)$ at the demodulation frequency F_e are given by

$$\widetilde{S}^2_{LOFI}(F_e, R_e, g) = 2R^2_{bs}\int_{-\infty}^{+\infty}\frac{PS_{LOFI}(2\pi F)}{\left|1 + G_{ofl}(2\pi F, g)\right|^2}\left|F_{int}\left[2\pi(F - F_e), T_{int}\right]\right|^2 dF \tag{19}$$

$$\widetilde{N}^2_{LOFI}\left(F_e, T_{int}, g\right) = 2R_{bs}\int_{-\infty}^{+\infty} \frac{PS_{noise}\left(2\pi F\right)}{\left|1+G_{ofl}\left(2\pi F, g\right)\right|^2}\left|F_{int}\left[2\pi\left(F-F_e\right), T_{int}\right]\right|^2 dF \tag{20}$$

where for an integration time T_{int} :

$$\left|F_{int}\left(\Omega, T_{int}\right)\right|^2 = \frac{1}{T_{int}^2}\frac{1}{\frac{1}{T_{int}^2}+\Omega^2} \tag{21}$$

is assumed to be a first order power filter.

By combining Eqs. (19) and (20) with Eq. (21), one finally obtains for a class-B laser ($F_R >> 1/\widetilde{\tau}_R\left(g\right)$) the following analytical expressions of the LOFI signal and of the LOFI noise:

$$\widetilde{S}^2_{LOFI}\left(F_e, R_e, g\right) = 2R^2_{bs}R_e\left(1-R_{bs}\right)^2 p^2_{out}\left|\widetilde{G}_{LOFI}\left(2\pi F_e, g\right)\right|^2 \tag{22}$$

$$N^2_{LOFI}\left(F_e, T_{int}, g\right) = R_{bs}p_{out}\frac{1}{2}\frac{\widetilde{\tau}_R\left(g\right)}{T_{int}}\left(\frac{1}{T_{int}}+\frac{1}{\widetilde{\tau}_R\left(g\right)}\right)\times\frac{\gamma_c^2}{\left[\frac{1}{T_{int}}+\frac{1}{\widetilde{\tau}_R\left(g\right)}\right]^2+\left[2\pi\left(F_e-F_R\right)\right]^2}. \tag{23}$$

Finally, by using Eqs. (22) and (23), one can determine the stationary LOFI SNR:

$$SNR\left(F_e, R_e, T_{int}, g\right) = \frac{S_{LOFI}\left(F_e, R_e, g\right)}{N_{LOFI}\left(F_e, T_{int}, g\right)}. \tag{24}$$

Fig. 2 shows the evolution of the stationary LOFI SNR (S_{LOFI}/N_{Laser}) versus the normalized shift frequency (F_e/F_R) for different values of the lock-in integration time (T_{int}) compared to the laser response time (τ_R). Fig. 2(a) shows that the stationary LOFI SNR (S_{LOFI}/N_{Laser}) is

frequency independent and above all shot noise limited for a laser with a short response time ($T_{\text{int}} >> \tau_R$):

$$\mathrm{SNR}\left(\mathrm{F_e}, \mathrm{R_e}, \mathrm{T_{int}} >> \tau_{\mathrm{R}}, \mathrm{g}\right) = \sqrt{\mathrm{R_e}}\left(1 - \mathrm{R_{bs}}\right) \times \sqrt{\mathrm{R_{bs}} \langle \mathrm{p_{out}} \rangle \mathrm{T_{int}}} \tag{25}$$

On the other hand, for a laser with a long response time ($T_{\text{int}} << \tau_R$), the stationary LOFI SNR is frequency dependent [Fig. 2(c)]. It is larger than the LOFI shot-noise limit, near the relaxation frequency and smaller than the LOFI shot-noise limit, far away from the relaxation frequency. More precisely we have already demonstrated in [20] that the LOFI SNR is larger (by a factor given by $\sqrt{\frac{\tau_R}{T_{\text{int}}}} > 1$) than the LOFI shot noise limit when working at the resonance frequency and lower (by a factor given by $\sqrt{\frac{T_{\text{int}}}{\tau_R}} < 1$) when working very far away from the resonance frequency. Therefore by controlling the effective laser response time $\tilde{\tau}_{\mathrm{R}}(\mathrm{g})$ by means of the electronic feedback loop, we are able to control the LOFI SNR.

Fig.2 also allows a comparison of the LOFI SNR obtained with two lasers having the same relaxation frequency, the same laser output power, but different laser response times.

As we can see, the LOFI SNR is higher, with the slowest laser (i.e. the laser with the longest response time) when working at the relaxation frequency and with the fastest laser (i.e. the laser with the shortest response time) when working far away from the relaxation frequency.

In the following of the present manuscript, only this last case has been experimentally study, because it corresponds to conventional condition for LOFI experiments ($\left|\mathrm{F_e} - \mathrm{F_R}\right| >> \Delta\Omega_{\mathrm{R}}/2\pi$) which allows to avoid saturation effects and also the signal perturbations induced by the laser

transient dynamics [20]. More precisely, our experimental study has been made by adjusting the frequency shift to: $F_e = 1.05 \times F_R$. Looking at Fig. 4, this frequency seems to be a good compromise between the conventional LOFI experimental condition mentioned above, the observation of a significant difference between the SNR of the lasers with the fast and the slow response time and also the measurement of sufficient SNR (>2), even for a short integration time [see Fig. 4(c)].

3. EXPERIMENTAL AND NUMERICAL RESULTS

A. The electronic feedback loop

To verify the stability of the electronic feedback loop, we have firstly evaluated the open loop gain $G_{ofl}(\Omega, g)$ which appears in the denominator of Eq. (11a). As explained previously [Eq. (9)], $G_{ofl}(\Omega, g)$ is the product of three different transfer functions, $G_{pump}(\Omega)$, the transfer function of the pump modulation, $G_{EFL}(\Omega)$, the transfer function of the electronic differentiator, and $G_{AOM}(\Omega)$ the transfer function of the AOM which controls the pumping power. By using a lock-in amplifier, gain and phase of the different transfer functions are experimentally determined for RF frequencies ($F = \Omega/2\pi$) between 100 kHz and 2.2 MHz. By fitting our experimental data, we have determined:

$$G_{pump}(\Omega) = \frac{\gamma_1 B I_S}{\Omega_R^2 - \Omega^2 + i\Omega\gamma_1 A} = \frac{\gamma_1}{\gamma_c} \frac{\Omega_R^2}{\Omega_R^2 - \Omega^2 + i\Omega\gamma_1 A} \tag{26a}$$

$$G_{AOM}(\Omega) = \exp(-i\Omega\tau_A) \tag{26b}$$

$$G_{EFL}(\Omega) = -\frac{i\Omega}{\Omega_c + i\Omega}\exp(-i\Omega\tau_E), \tag{26c}$$

with: $\frac{\gamma_1}{\gamma_c} \approx 5\times10^{-6}$, $\Omega_R = 2\pi\times 950\,\text{kHz}$, $\Delta\Omega_R = \gamma_1 A \approx 4\times10^4\,\text{s}^{-1}$, $\tau_A = 1.55\,\mu\text{s}$, $\Omega_c = 2\pi\times 1750\,\text{kHz}$ and $\tau_E = 0.125\,\mu\text{s}$.

By looking at the above parameters, one can notice, that our free running laser is a class-B laser ($\Omega_R >> \Delta\Omega_R$), with a high LOFI gain ($G_{LOFI}(\Omega_R) \propto \frac{\gamma_c}{\gamma_1} >> 1$) and with a relaxation frequency below the cut-off frequency of the electronic differentiator ($\Omega_R < \Omega_c$). In Eq. (26c), the electronic time delay τ_E, is principally due to the electric links, before, inside (mainly the operational amplifier) and after the electronic differentiator. This time delay induces a relatively small phase shift in the feedback loop ($\Omega_R\tau_E = 0.75 = \pi\times 0.24$). On the other hand, the acoustic time delay τ_A is much longer. It is the time needed by the acoustic wave to go from the electrode of the AOM to the laser pump beam inside the quartz crystal. This long time delay induces a larger phase shift, depending on the pump beam position in the AOM ($6.0 = \pi\times 1.9 \le \Omega_R\tau_A \le 14.9 = \pi\times 4.8$). To compensate for these phase shifts, the AOM position has been adjusted to $\tau_A = 1.55\,\mu\text{s}$, so that $\Omega_R(\tau_E + \tau_A) \approx 3\pi$. A minus sign has also be added in the electronic differentiator [compare Eq. (26c) with Eq. (14)], by simply inverting its output voltage, to finally obtain: $-\exp[j\Omega_R(\tau_E + \tau_A)] \approx 1$.

In Eq. (9), the proportionality constant gR_{bs} allows to take into account all the optical losses and the electronic amplifications (or attenuations) which occur in the loop. When working with the

best experimental conditions to obtain a stable and robust loop, we have experimentally determined:

$$gR_{bs} \approx 5 \times 10^4 \tag{26d}$$

At this point, using Eq. (17) and improperly Eq. (18) obtained for a perfect differentiator, one can estimate the response time of the free running laser, $\tau_R \approx 50\,\mu s$, and of the laser controlled by the stable loop using a perfect differentiator, $\tilde{\tau}_R(g) \approx 2.4\,\mu s$. By using the electronic feedback loop, we can therefore expect to decrease the laser response time by a factor with a maximum value of 20.

Figs 3(a) and 3(b) show the experimental Bode diagrams of the open loop gain (gain and phase versus frequency). As we can see, the electronic feedback loop principally acts at the laser relaxation frequency and in its vicinity, and the experimental results agree with the product of the fitted transfer function given, by Eqs. (26). As it is well known in the standard theory of electronic control, the maximum phase shift at the two unity gain points has to be less than 2π in order to have a stable feedback loop [27,28]. This task which is naturally difficult to realize because of the relaxation oscillations that introduce a π phase shift, is further complicated in our case, due to the relatively high value of the relaxation frequency of the microchip lasers which lies in the megahertz range (in contrast with the usual kilohertz range for the standard laser cavities). The bode diagram is a useful tool in designing the electronic control loop [27,28], however, it does not easily show us the stability of the loop mentioned above. On the other hand, the Nyquist diagram (imaginary part of the open loop gain versus its real part, for different frequencies) allows us to analyze the stability in a simpler way. Figs 3(c) and 3(d) show that the

instability point $(-1,0)$ is not circled by the loop, hence the loop is stable. It also shows that the loop is very near the instability point and enters the unity circle [only shown on Fig. 3(d)] around the instability point, for different frequencies and consequently there will be a noise increase for these frequencies. The stability of our loop is rather critical and this prevents one from using a larger value of the open feedback loop gain, i.e. a higher value of g [see Eq. (9)].

Now we present the experimental results obtained with our Nd microchip laser operating with the feedback loop described previously. Fig. 4 shows the dynamical behavior of the free running laser ($g = 0$) and of the laser controlled by the electronic feedback loop ($g \neq 0$). The comparison of Figs. 4(a) and 4(b) shows how the temporal behavior of the laser is stabilized by the electronic feedback loop. Indeed, one can observe a significant reduction of the laser temporal fluctuations. Figs. 4(c) and 4(d) show the corresponding RF power spectrum. In agreement with the Bode diagram, one can see that the electronic feedback loop mainly acts at the laser relaxation frequency and its vicinity. Indeed, when reducing the height of the power spectrum, one can observe an increase of the resonance width, which finally corresponds to a reduction of the laser response time.

In these figures, the experimental noise power spectra have been adjusted by using Eq. (12) with $R_e = 0$ and respectively, $G_{ofl}(\Omega, g = 0) = 0$ for the free running laser [Fig. 4(c)] and $G_{ofl}(\Omega, g \neq 0) \neq 0$ for the controlled laser [Fig. 4(d)]. In Fig. 4(c), the discrepancies between the analytical and experimental curves, at low and high frequencies, come respectively from polarization mode coupling [29,30] and nonlinear noise laser dynamics, not included in our analytical development of Sec. II B [27]. Nevertheless, Fig. 4(c) allows us to determine the free laser dynamics parameters: $\Omega_R \approx 2\pi \times 950\,\text{kHz}$ and $\tau_R \approx 50\,\mu\text{s}$.

One can see in Fig. 4(d), that the noise power spectrum of the controlled laser has been adjusted two times. Firstly, by using the real feedback loop, where $G_{ofl}(\Omega, g)$ is defined by using Eqs. (26) and secondly by using an ideal feedback loop (corresponding to an ideal differentiation), where $G_{ofl}(\Omega, g)$ leads to Eq.(15). In the real case, one can observe a good (but not perfect) agreement between the experimental result and the analytical prediction. As mentioned previously, the difference can be explained by the fact that our loop is very near the instability point and that its stability is rather critical [27,28]. Finally, using Eq. (18), the ideal case allows us to determine, the response time of the controlled laser: $\tilde{\tau}_R(g) \approx 3\,\mu s$. As expected, this time is shorter than the response time of the free running laser: $\tilde{\tau}_R(g) \approx \tau_R/17$. This laser response time is the shortest that we have been able to obtain with our electronic feedback loop. As already mentioned, this technical limit comes from the critical stability of our feedback loop, which prevents one from using a larger value of the open feedback loop gain, i.e. a higher value of g [see Eq. (9)]. At this point, one can notice that the obtained minimum value of $\tilde{\tau}_R(g) \approx 3\,\mu s$ is very far away the physical limit of the LOFI method.

Indeed, as it is already explained in [20], the shortest possible value of the laser response time is given by:

$$\tau_{R,opt} = \left(\frac{2}{\gamma_1 r}\right)_{opt} = \frac{2}{\sqrt{2R_{bs}}} \frac{NEP/(hc/\lambda)}{\gamma_c \sqrt{\langle p_{out} \rangle}}, \tag{27}$$

Where the detection noise level is characterized by its noise equivalent power: NEP ($W/\sqrt{Hz}$),For example, for a laser with an output power $P_{out} = 10\,mW$ ($\langle p_{out} \rangle = 5 \times 10^{16}$ photons/s at $\lambda = 1064\,nm$), a cavity damping rate $\gamma_c = 5 \times 10^9\,s^{-1}$ and for a

setup with a beam splitter reflectivity $R_{bs} = 0.5$ and a noise equivalent power $NEP = 6 \times 10^{-9}\ W/\sqrt{Hz}$, one obtains finally $\tau_{R,opt} \approx 58\,ns \approx \tilde{\tau}_R(0)/1000$. With our feedback loop we are therefore very far the ultimate limit of the LOFI method.

Finally, one can also observe on Fig. 4(d) an experimental increase (by comparison with the case of the ideal feedback loop) of the noise on the left shoulder of the noise power spectrum (typically in the vicinity of $F/F_R = 0.8$). As previously mentioned, this noise excess comes from the fact that our feedback loop enters the unity circle around the instability point [see Fig. 3(d)].

B. LOFI images with an electronic feedback loop

To show the effect of the electronic feedback loop on LOFI imaging, we have compared 1D scans obtained for different experimental conditions (i.e. for different values of the integration time T_{int} compared with the laser response time $\tilde{\tau}_R(g)$. More precisely, we have compared in Fig. 5, the LOFI signals obtained by using the free running laser ($g = 0$), with a laser response time: $\tilde{\tau}_R(0) = \tau_R = 50\,\mu s$, and by using the controlled laser ($g \neq 0$), with a shorter response time: $\tilde{\tau}_R(g) \approx 3\,\mu s$. The two lasers have the same output power ($\langle p_{out} \rangle$) and the same relaxation frequency (F_R). Here, our aim is to determine the best laser, for high quality imaging (i.e. large LOFI SNR). Our study has been made outside the resonance frequency ($F_e \neq F_R$), which corresponds to typical experimental conditions to avoid LOFI saturation effect and also the perturbations induced by the laser transient dynamics [18-20].

Fig.5 shows a comparison between numerical (left column) and experimental (right column) results. The numerical results have been obtained by using a Runge-Kutta method to solve the set of differential equations (1). The target under investigation is a reflectivity slab with $R_e \neq 0$ only in the central part of the 1D scans (pixel 26 to 50). For the current numerical study, the value of the effective reflectivity ($R_e = 4 \times 10^{-10}$) has been chosen to obtain a good agreement between the experimental and the numerical results. Moreover, this very low value allows studying the LOFI sensitivity under ultimate conditions: $R_e \times (1 - R_{bs})^2 \times p_{out} \approx 5 \times 10^6$ photons/s (≈ 0.06 pW), i.e. near the shot noise limit, for the shortest integration time ($R_e \times (1 - R_{bs})^2 \times p_{out} \times 5\mu s \approx 2$ *photons*).

For the experimental study, the target under investigation is a diffusive object. To avoid any signal fluctuation induced by some differences between the effective reflectivity of two adjacent points of the target, the focal spot of the beam is kept fixed on the target. Then, the reflectivity slab is simulated by using a mechanical chopper in front of the diffusive target. The experimental scan is therefore a temporal scan (i.e. a virtual scan compared to a conventional spatial scan) where the beam position is kept fixed and the target reflectivity is time dependent due to the mechanical chopper.

Although the experimental scan is virtual, one can observe on Fig. 5 a similarity between the experimental and the numerical graphs. The results of Fig. 5 also show, a good agreement with the theoretical predictions [Eq. (25) and the resulting Fig. 2]. Indeed, whatever the integration time, the LOFI SNR is always better (i.e. the reflectivity slab is easier to see) when we work with the laser controlled by our electronic feedback loop (i.e. with the laser having the shortest response time). The quality difference (i.e. the SNR) between the 1D images obtained

with the two lasers is much more important when the integration time is short (i.e. when the imaging speed is fast).

Table 1 shows the LOFI SNR obtained from the numerical and the experimental results of Fig. 5. For comparison, this table also gives the LOFI SNR analytically calculated from Eq. (24) and the corresponding shot noise limit [Eq. (25)].

As we can see, the LOFI SNR obtained with the controlled laser (i.e. with $\tilde{\tau}_R(g) \approx 3\mu s$) is always higher than the LOFI SNR obtained with the free running laser (i.e. with $\tau_R \approx 50\mu s$). One can also point out that with the controlled laser, the experimental condition: $T_{int} \geq \tilde{\tau}_R(g)$ is satisfied, and therefore the LOFI SNR is near the shot noise limit. On the other hand, with the controlled laser, one has: $T_{int} \leq \tau_R$, and the LOFI SNR is always below the shot noise limit.

Even if the result of table 1 seems to less significant than the visual effect given by the observation of Fig. 5, one can finally conclude that when the laser response time is shorter, the image quality can be better (i.e. the LOFI SNR can be higher). Therefore, the use of an adapted electronic feedback loop can allow high speed LOFI Imaging (i.e. imaging with a short integration time) with a shot-noise limited sensitivity, when working under typical LOFI experimental conditions (i.e. $F_e \neq F_R$)

To confirm the previous results, but this time with a conventional spatial scan of the laser beam on the target (i.e. not a virtual temporal scan with a mechanical chopper), Fig. 6 shows two LOFI images of the edge of a metallic ruler. The first one is obtained with the free running laser and the second one with the laser controlled by the electronic feedback loop. One can easily observe that the SNR obtained with the controlled laser ($SNR_b \approx 17dB$) is higher than the SNR obtained with the free running laser ($SNR_a \approx 11dB$). The effective reflectivity of the ruler is

estimated to be: $\langle R_e \rangle \approx 2 \times 10^{-10}$, which corresponds to the detection of: $R_e \times (1 - R_{bs})^2 \times p_{out} \times 50\,\mu s \approx 160$ photons for each pixel of the bright part of the ruler.

5. CONCLUSION

In a LOFI setup, the beating between the reference beam and the signal beam takes place inside the laser cavity and therefore the laser fulfills simultaneously the roles of emitter and detector of photons. In these conditions, the laser relaxation oscillations play a leading role both in the laser quantum noise which determines the SNR and in the laser transient dynamics which determines the response time of the LOFI setup. In the present study, we have experimentally compared the stationary LOFI SNR of two lasers. The first one is a free running microchip laser while the second one is the same laser, dynamically controlled by an electronic feedback loop. More precisely, by using an electronic differentiator acting on the pumping power by the way of an AOM, the pumping power decreases (respectively increases) when the laser power increases (respectively decreases), which stabilizes the laser power fluctuations. Experimentally, the use of an electronic differentiator allows the comparison between two kinds of lasers. The free running laser, when the feedback loop is off (i.e. inactive), and the dynamically controlled laser, when the feedback loop is on (i.e. active). Thanks to the use of a differentiator, the two studied lasers have the same average output power and the same relaxation frequency, but have two different response time values.

Firstly, we have analytically shown that the LOFI SNR is higher with the slowest laser (i.e. the laser with the longest response time) when working at the relaxation frequency or with the fastest laser (i.e. the laser with the shortest response time) when working far away from the relaxation

frequency. Therefore, by controlling the effective laser response time $\tilde{\tau}_R(g)$ with the electronic feedback loop, we are able to control the LOFI SNR.

Secondly, using a Nyquist diagram, we have experimentally shown that our electronic feedback loop using an electronic differentiator is stable, but rather critical. This limits the open loop gain value and consequently, the laser response time can only be decreased by a factor with a maximum value of the order of 20 ($\tilde{\tau}_R(g) \approx \tilde{\tau}_R(0)/20$). This laser response time is the shortest that we have been able to obtain due to the critical stability of our electronic feedback loop. The obtained response time is still far away the physical limit of the LOFI method.

Despite this technical limit, LOFI images (1D and 2D) obtained with and without the electronic feedback loop have been compared to determine the best laser conditions for high quality imaging (i.e. large LOFI SNR). To avoid LOFI saturation effect and also the perturbations induced by the laser transient dynamics, our experimental study has been made, not at the relaxation frequency, but in its neighborhood ($F_e = 1.05 \times F_R$) which roughly corresponds to conventional LOFI experimental condition. In agreement with the analytical predictions, our experimental study clearly shows that whatever the lock-in integration time, the LOFI SNR is always better when using the laser controlled by the electronic feedback loop i.e. the laser with the shortest laser response time.

One can also notice that with the controlled laser, the experimental condition: $T_{int} \geq \tilde{\tau}_R(g)$ is satisfied and therefore the LOFI SNR is near the shot noise limit while for the free running laser, one has: $T_{int} \leq \tau_R$ and the LOFI SNR is always lower than the shot noise limit.

One can finally conclude that when the laser response time is shorter, the image quality can be better (i.e. the LOFI SNR can be higher). Therefore, the use of an adapted electronic feedback loop can allow high speed LOFI Imaging (i.e. imaging with a short integration time)

with a shot-noise limited sensitivity, when working under typical LOFI experimental conditions (i.e. $F_e \neq F_R$).

REFERENCES

1. T. Yoshizawa, editor, Handbook of optical metrology: Principles and Applications (CRC Press, 2009).
2. K. Otsuka, "Effects of external perturbations on $LiNdP_40_{12}$ Lasers," IEEE J. Quantum Electron., **QE-15**, 655-663 (1979).
3. K. Otsuka, "Self-Mixing Thin-Slice Solids-State Laser Metrology," Sensors 11, 2195-2245 (2011).
4. K. Otsuka, "Highly sensitive measurement of Doppler-shift with a microchip solid-state laser," Jpn. J. Appl. Phys. **31,** L1546–L1548 (1992).
5. S. Okamoto, H. Takeda, and F. Kannari, "Ultrahighly sensitive laser-Doppler velocity meter with a diode-pumped Nd:YVO4 microchip laser," Rev. Sci. Instrum. **66,** 3116–3120 (1995).
6. R. Kawai, Y. Asakawa, K. Otsuka, "Ultrahigh-Sensitivity Self-Mixing Laser Doppler Velocimetry with Laser-Diode-Pumped Microchip $LiNdP_4O_{12}$ Lasers," IEEE Photonics Technology Lett. **11**, 706-708 (1999).
7. S. Suddo, T. Ohtomo, Y. Takahascvhi, T. Oishi, K. Otsuka, "Determination of velocity of self-mobile phytoplankton using a self thin-slice solid–state laser," Appl. Opt. **48**, 4049-4055 (2009).
8. K. Otsuka, K. Abe, J.Y. Ko, and T.S. Lim, "Real-time nanometer vibration measurement with self-mixing microchip solid-state laser," Opt. Lett. **27**, 1339-1341 (2002).

9. V. Muzet, E.Lacot, O. Hugon, Y. Gaillard, “Experimental comparison of shearography and laser optical feedback imaging for crack detection in concrete structures,” Proc. SPIE 5856, 793-799 (2005).
10. E. Lacot, and O. Hugon, “Phase-sensitive laser detection by frequency-shifted optical feedback,” Phys. Rev. A **70,** 053824 (2004).
11. H. Gilles, S. Girard, M. Laroche, and A. Belarouci, “Near-field amplitude and phase measurements using heterodyne optical feedback on solid-state lasers,” Opt. Lett. **33**, 1-3 (2008).
12. S. Blaize, B. Bérenguier, I. Stéfanon, A. Bruyant, G. Lerondel, P. Royer, O. Hugon, O. Jacquin, and E. Lacot, “ Phase sensitive optical near-field mapping using frequency-shifted laser optical feedback interferometry,” Opt. Express **16**, 11718-11726 (2008).
13. E. Lacot, R. Day, and F. Stoeckel, “Laser optical feedback tomography,” Opt. Lett. **24,** 744–746 (1999).
14. A. Witomski, E. Lacot, O. Hugon, and O. Jacquin, “Synthetic aperture laser optical feedback imaging using galvanometric scanning,” Opt. Lett. **31**, 3031-3033 (2006).
15. O. Hugon, I.A. Paun, C. Ricard, B. van der Sanden, E. Lacot, O. Jacquin, A. Witomski, “Cell imaging by coherent backscattering microscopy using frequency shifted optical feedback in a microchip laser,” Ultramicroscopy **108**, 523-528 (2008).
16. O. Hugon, F. Joud, E. Lacot, O. Jacquin, H. Guillet de Chatellus, Coherent microscopy by laser optical feedback imaging (LOFI) technique, Ultramicroscopy (2011) doi: 10.1016/j.ultramic.2011.08.004.
17. E. Lacot, R. Day, and F. Stoeckel, “Coherent laser detection by frequency-shifted optical feedback,” Phys. Rev. A **64,** 043815 (2001).

18. E. Lacot, O. Jacquin, G. Roussely, O. Hugon, H. Guillet de Chatellus, “Comparative study of autodyne and heterodyne laser interferometry for imaging,” J. Opt. Soc. Am. A **27**, 2450-2458 (2010).
19. O. Jacquin, E. Lacot, W. Glastre, O. Hugon, H. Guillet de Chatellus, “Experimetal comparison of autodyne and heterodyne laser interferometry using an Nd:YVO4 microchip laser,” J. Opt. Soc. Am. A **28**, 1741-1746 (2011).
20. E. Lacot, W. Glastre, O. Jacquin, O. Hugon, H. Guillet de Chatellus, “Optimization of an autodyne laser interferometer for high speed confocal imaging,” J. Opt. Soc. Am. A **30**, 60-70 (2013).
21. J.J. Zaykowski and A. Mooradian, “Single –frequency microchip Nd lasers,” Opt. Lett. **1**, 24-26 (1989).
22. M.I. Kolobov, L. Davidovich, E. Giacobino, and C. Fabre, “Role of pumping statistics and dynamics of atomic polarization in quantum fluctuations of laser sources,” Phys. Rev. A **47**, 1431-1446 (1993).
23. A. Bramati, J.P. Hermier, V. Jost, E. Giacobino, L. Fulbert, E. Molva, and J.J. Aubert, “Effects of pump fluctuations on intensity noise of Nd:YVO4 microchip lasers,” Eur. Phys. J. D. **6**, 513-521 (1999).
24. Y.I. Khanin, Principles of laser dynamics, (Elsevier, 1995).
25. Experimentally, the minus sign comes directly from the fact that when the RF voltage applied on the AOM increases, the intensity of the zero order beam of the AOM decreases and therefore the pumping power decreases.

26. On Fig.1, this complex gain (amplitude and phase) is the ratio between the input voltage applied on the AOM, and the output voltage of the electronic differentiator, when the link between these two component is open (i.e. no direct connection)
27. A. Bramati, J.-P. Hermier, V. Jost, E. Giacobino, "Feedback control and nonlinear intensity noise of Nd:YVO4 microchip lasers," Phys. Rev. A **62**, 043806 (2000).
28. C.C. Harb, M.B. Gray, H.-A Bachor, R. Schilling, P. Rottengatter, I. Freitag, H. Welling, "Suppression of the Intensity Noise in a Diode-Pumped Neodymium YAG Nonplanar Ring Laser," IEEE J. Quantum Electron. **30**, 2907-2913 (1994).
29. S. Bielawski, D. Derozier, P. Glorieux, "Antiphase dynamics and polarization effects in the Nd-doped fiber laser," Phys. Rev. A **46**, 2812-2822 (1988).
30. E. lacot, F. Stoeckel, "Nonlinear mode coupling in a microchip laser," J. Opt. Soc. Am. B **13**, 2034-2040 (1996).

FIGURE CAPTIONS

Fig. 1. Schematic diagram of the LOFI setup with an electronic feedback loop using a differentiator. L_1, L_2 , L_3, L_4 and L_5: Lenses, AOM: Acousto-Optic Modulator, BS: Beam Splitter with a power reflectivity R_{bs}, GS: Galvanometric Scanner, FS Frequency Shifter with a round trip frequency-shift F_e, PD: Photodiode. The lock-in amplifier is characterized by its integration time T_{int}. The Nd^{3+}: microchip-laser is characterized by its output power p_{out} (photons/s), its relaxation frequency F_R and its dynamical response time τ_R. The optical feedback from the target is characterized by the effective reflectivity $R_e << 1$.

Fig. 2. Stationary LOFI SNR (S_{LOFI}/N_{Laser}) versus the normalized shift-frequency (F_e/F_R) for different values of the lock-in integration time: a) $T_{int} = 500\mu s$, b) $T_{int} = 50\mu s$, c) $T_{int} = 5\mu s$. For each integration time, the dotted line and the solid line show the exact value of the LOFI SNR [Eq. (24)], when respectively $\tau_R = 50\mu s$ and $\tau_R = 3\mu s$, while the dashed line shows the corresponding LOFI shot-noise limit [Eq. (25)]. The calculation conditions are: $R_e = 4\times10^{-10}$ and $R_{bs} = 1/2$. The laser is a class-B laser with: $p_{out} \approx 5\times10^{16}\ photons/s$ ($P_{out} \approx 10\,mW$ at $\lambda = 1064$ nm) and $F_R = 950$ kHz . The vertical dash-dotted line ($F_e = 1.05\times F_R$) corresponds to the working frequency for the remainder of this manuscript.

Fig. 3. Open-loop transfer function $[G_{ofl}(F_e)]$: (a) Bode diagram for the gain (i.e. the modulus); (b) Bode diagram for the phase; (c) Nyquist diagram in the complex plane; (d) Zoom of the left part of the Nyquist diagram near the instability point $[\times(-1,0)]$. ○: experimental results; Solid lines: fitted transfer function; Dashed line: unity circle around the instability point.

Fig. 4. Dynamical behavior of the free running laser (left column: Figs. (a) and (c)) and of the laser with the electronic feedback control (right column: Figs. (b) and (d)). Top row: temporal behavior; Bottom row: corresponding RF power spectra with $F_R \approx 950$kHz .The RF power spectra are fitted by using [Eq. (12)] with $R_e = 0$. Fig. 4(c), dashed line: $G_{ofl} = 0$, i.e. no feedback loop, $\tau_R \approx 50\mu s$. Fig. 4(d): dashed line: $G_{ofl} \neq 0$ and calculated with the parameter of the ideal feedback loop, $\tilde{\tau}_R(g) \approx 3\mu s$. Fig. 3(d), dash-dotted line: $G_{ofl} \neq 0$ calculated with the parameter of the real feedback loop, i.e. experimentally determined) [Eqs. 26].

Fig. 5. Numerical (left column) and experimental (right column) 1D LOFI scans, for different values of the lock-in integration time: a) & e) $T_{int} = 50\mu s$, b) & f) $T_{int} = 20\mu s$, c) & g) $T_{int} = 10\mu s$, d) & h) $T_{int} = 5\mu s$. Curves with circles (○): results obtained with the free running laser (i.e. $\tau_R \approx 50\mu s$); Solid curves results obtained with the electronic feedback control (i.e. $\tau_R \approx 3\mu s$). Experimental conditions: $P_{out} \approx 10\,mW$ (i.e. $p_{out} \approx 5\times10^{16}\ photons/s$ at $\lambda = 1064\,nm$); $F_R \approx 950$kHz ; $F_e \approx 1.05\times F_R$; $R_{bs} = 0.5$; the target is a reflectivity block with

$R_e = 0$ (pixels 1-25 & 51-70) and $R_e \approx 4 \times 10^{-10}$ (pixels 26-50) with $R_e \times (1 - R_{bs})^2 \times p_{out} \approx 5 \times 10^6 \; photons/s \approx 0.06 \, pW$.

Fig. 6. LOFI images of the edge of a metallic ruler. (a) image obtained with the free running laser (i.e. $\tau_R \approx 50 \mu s$) and giving a signal to noise ratio of: $SNR_a \approx 11 dB$; (b) image obtained with the laser controlled by the electronic feedback loop (i.e. $\tau_R \approx 3 \mu s$) and giving $SNR_b \approx 17 dB$. Experimental conditions: $P_{out} \approx 10 mW$ (i.e. $p_{out} \approx 5 \times 10^{16} \; photons/s$ at $\lambda = 1064 nm$), $F_R \approx 950 kHz$; $F_e \approx 1.05 \times F_R$; $R_{bs} = 0.5$ and $T_{int} = 50 \mu s$. The SNR have been calculated by dividing the mean values of the measured signals on the ruler (right rectangle) and outside the ruler (left rectangle). The effective reflectivity of the ruler is estimated to be : $\langle R_e \rangle \approx 2 \times 10^{-10}$, which corresponds to the detection of: $R_e \times (1 - R_{bs})^2 \times p_{out} \times 50 \mu s \approx 160$ photons for each pixel of the bright part of the ruler.

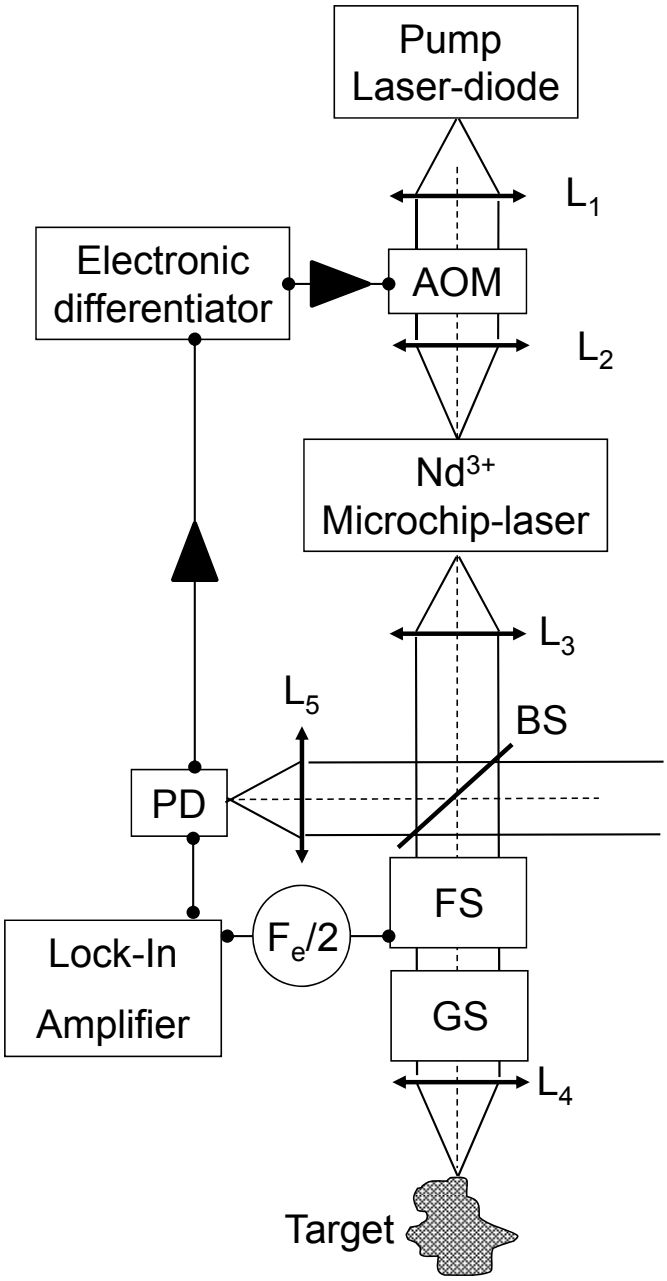

Fig. 1. Schematic diagram of the LOFI setup with an electronic feedback loop using a differentiator. L_1, L_2 , L_3, L_4 and L_5: Lenses, AOM: Acousto-Optic Modulator, BS: Beam Splitter with a power reflectivity R_{bs}, GS: Galvanometric Scanner, FS Frequency Shifter with a round trip frequency-shift F_e, PD: Photodiode. The lock-in amplifier is characterized by its integration time T_{int}. The Nd^{3+}: microchip-laser is characterized by its output power p_{out} (photons/s), its relaxation frequency F_R and its dynamical response time τ_R. The optical feedback from the target is characterized by the effective reflectivity $R_e << 1$.

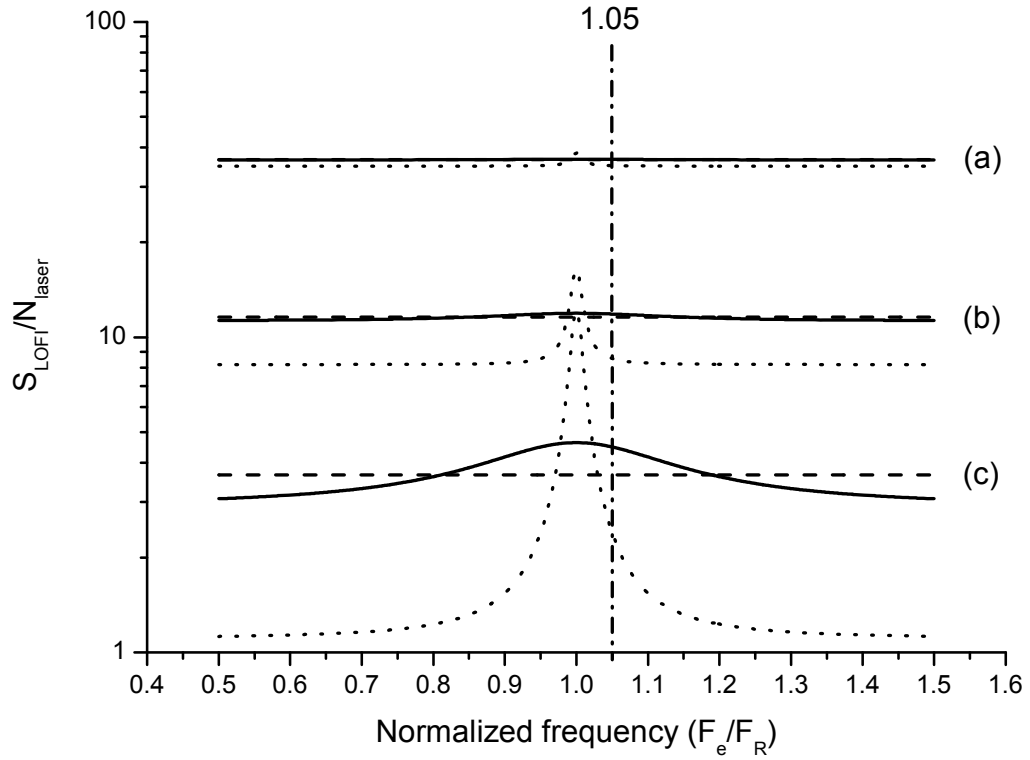

Fig. 2. Stationary LOFI SNR (S_{LOFI}/N_{Laser}) versus the normalized shift-frequency (F_e/F_R) for different values of the lock-in integration time: a) $T_{\text{int}} = 500\,\mu s$, b) $T_{\text{int}} = 50\,\mu s$, c) $T_{\text{int}} = 5\,\mu s$. For each integration time, the dotted line and the solid line show the exact value of the LOFI SNR [Eq. (24)], when respectively $\tau_R = 50\,\mu s$ and $\tau_R = 3\,\mu s$, while the dashed line shows the corresponding LOFI shot-noise limit [Eq. (25)]. The calculation conditions are: $R_e = 4\times10^{-10}$ and $\mathrm{R_{bs}} = 1/2$. The laser is a class-B laser with: $p_{out} \approx 5\times10^{16}\ photons/s$ ($P_{out} \approx 10\,mW$ at $\lambda = 1064\,\mathrm{nm}$) and $\mathrm{F_R} = 950\,\mathrm{kHz}$. The vertical dash-dotted line ($F_e = 1.05\times F_R$) corresponds to the working frequency for the remainder of this manuscript.

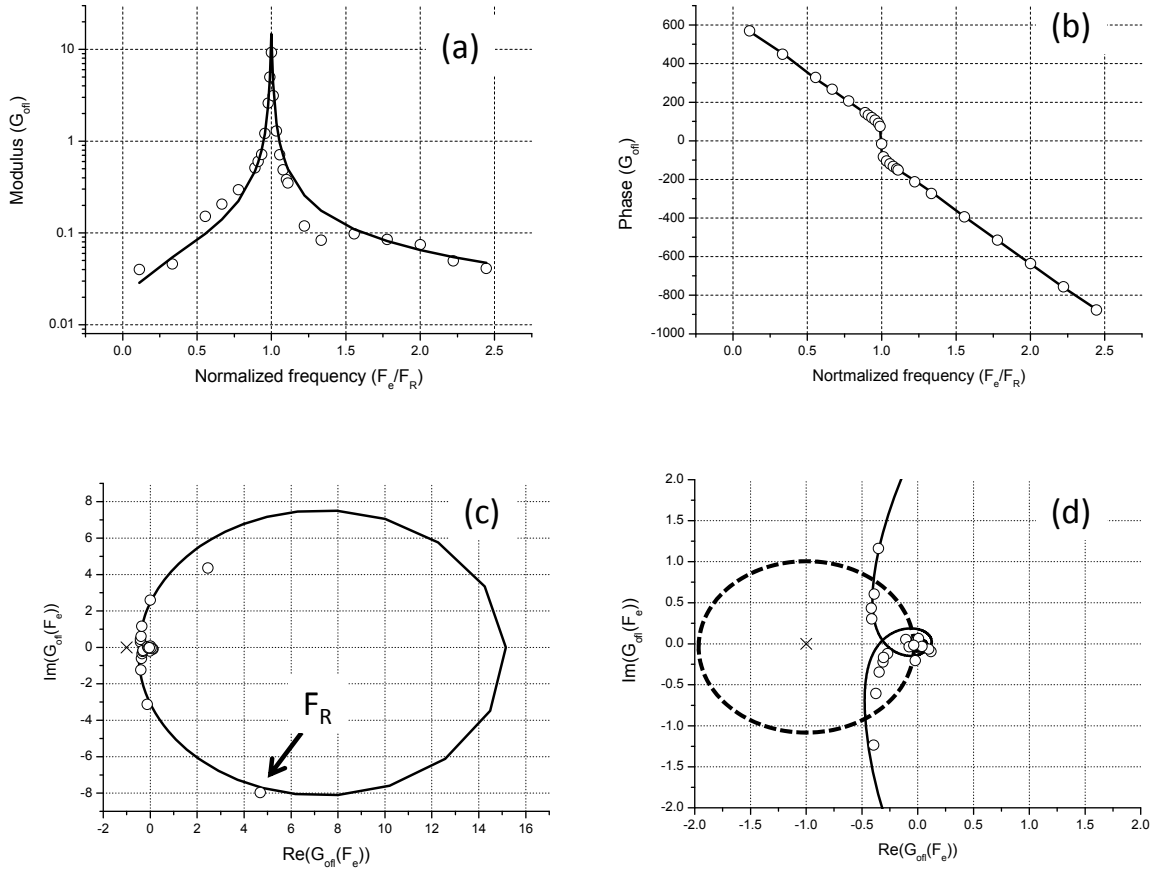

Fig. 3. Open-loop transfer function $[G_{ofl}(F_e)]$: (a) Bode diagram for the gain (i.e. the modulus); (b) Bode diagram for the phase; (c) Nyquist diagram in the complex plane; (d) Zoom of the left part of the Nyquist diagram near the instability point $[\times(-1,0)]$. ○: experimental results; Solid lines: fitted transfer function; Dashed line: unity circle around the instability point.

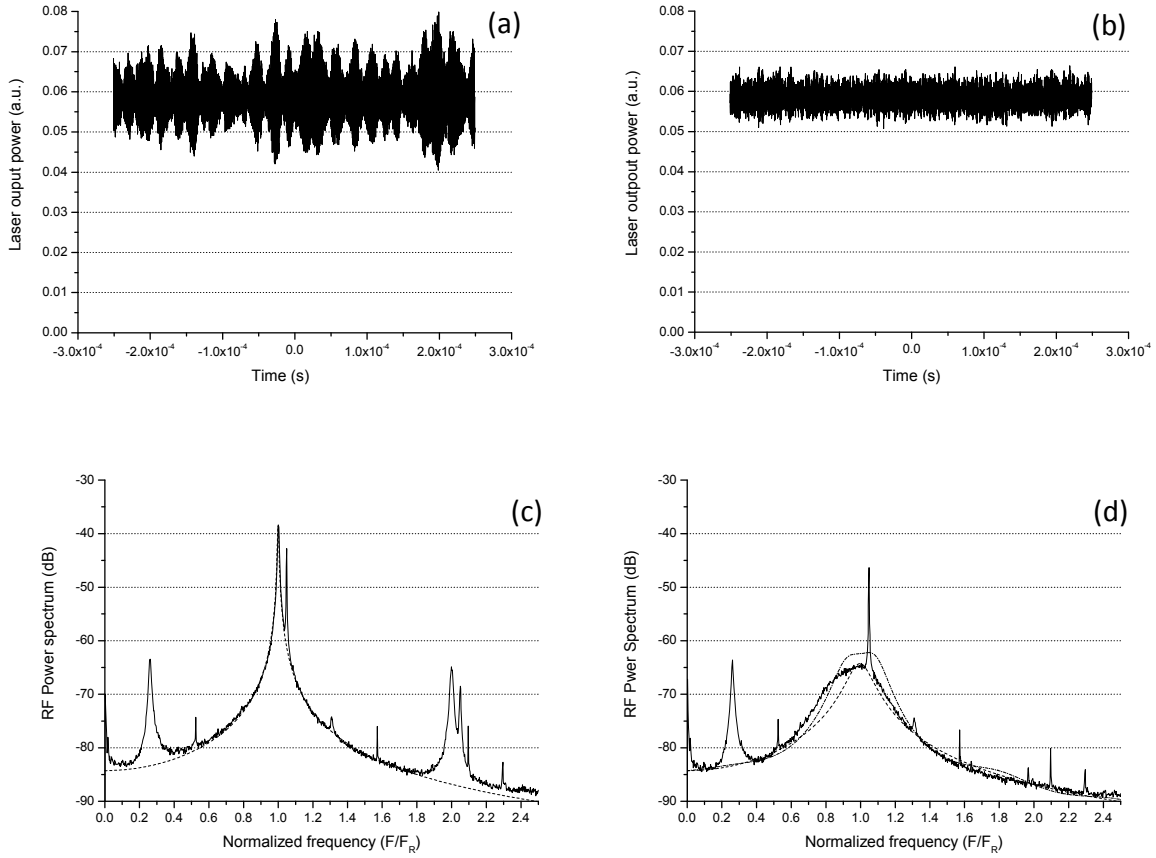

Fig. 4. Dynamical behavior of the free running laser (left column: Figs. (a) and (c)) and of the laser with the electronic feedback control (right column: Figs. (b) and (d)). Top row: temporal behavior; Bottom row: corresponding RF power spectra with $F_R \approx 950\,\mathrm{kHz}$.The RF power spectra are fitted by using [Eq. (12)] with $R_e = 0$. Fig. 4(c), dashed line: $G_{ofl} = 0$, i.e. no feedback loop, $\tau_R \approx 50\,\mu\mathrm{s}$. Fig. 4(d): dashed line: $G_{ofl} \neq 0$ and calculated with the parameter of the ideal feedback loop, $\tilde{\tau}_R(g) \approx 3\,\mu\mathrm{s}$. Fig. 3(d), dash-dotted line: $G_{ofl} \neq 0$ calculated with the parameter of the real feedback loop, i.e. experimentally determined) [Eqs. 26].

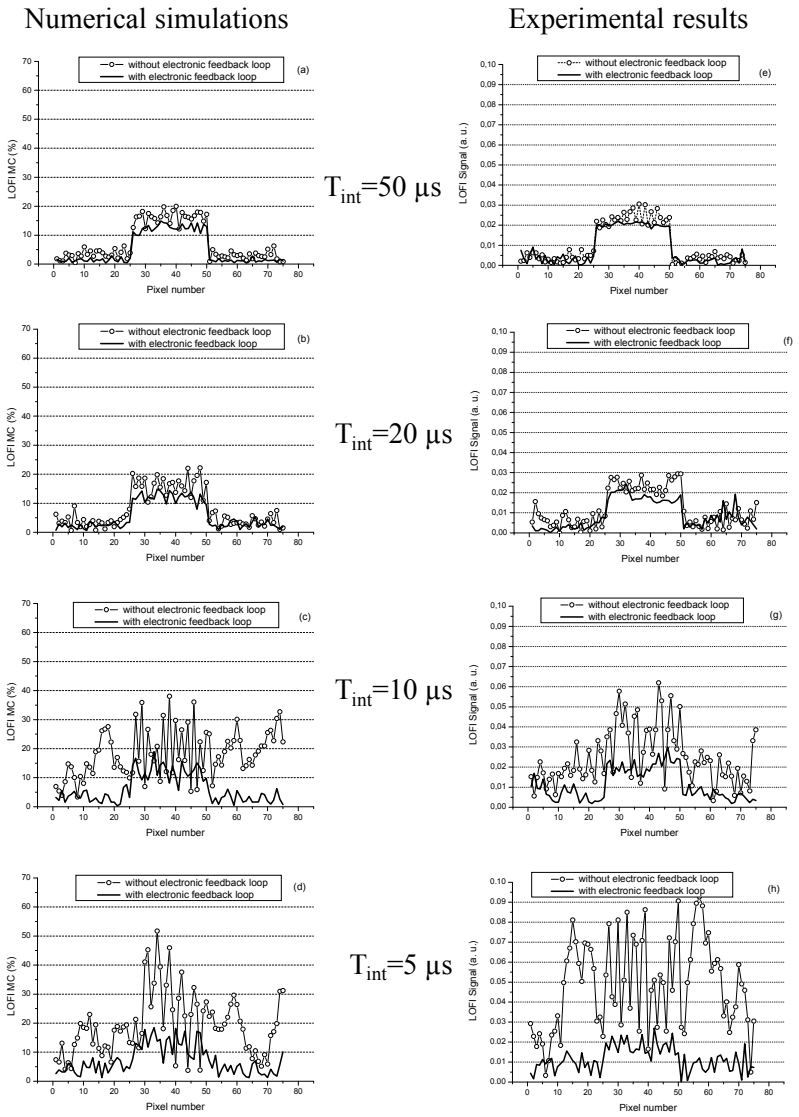

Fig. 5. Numerical (left column) and experimental (right column) 1D LOFI scans, for different values of the lock-in integration time: a) & e) $T_{\text{int}} = 50\mu s$, b) & f) $T_{\text{int}} = 20\mu s$, c) & g) $T_{\text{int}} = 10\mu s$, d) & h) $T_{\text{int}} = 5\mu s$. Curves with circles (O): results obtained with the free running laser (i.e. $\tau_R \approx 50\mu s$); Solid curves results obtained with the electronic feedback control (i.e. $\tau_R \approx 3\mu s$). Experimental conditions: $P_{out} \approx 10mW$ (i.e. $p_{out} \approx 5\times10^{16}\ photons/s$ at $\lambda = 1064\,nm$); $\mathrm{F_R} \approx 950\,\mathrm{kHz}$; $F_e \approx 1.05\times F_R$; $\mathrm{R_{bs}} = 0.5$; the target is a reflectivity block with $R_e = 0$ (pixels 1-25 & 51-70) and $R_e \approx 4\times10^{-10}$ (pixels 26-50) with $R_e \times (1-R_{bs})^2 \times p_{out} \approx 5\times10^6\ photons/s \approx 0.06\,pW$.

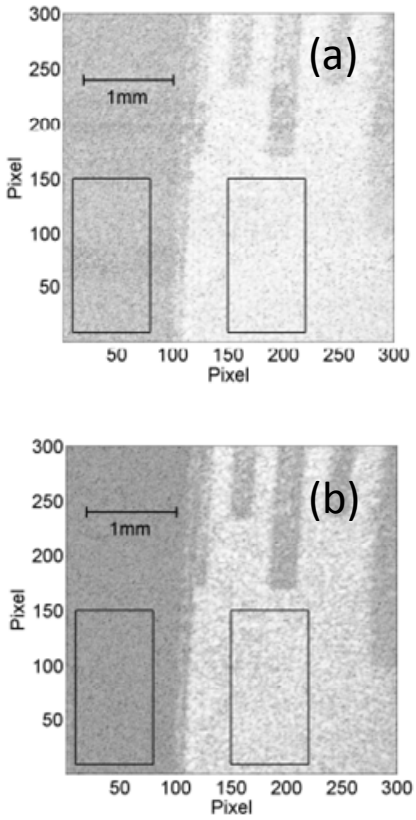

Fig. 6. LOFI images of the edge of a metallic ruler. (a) image obtained with the free running laser (i.e. $\tau_R \approx 50\mu s$) and giving a signal to noise ratio of: $SNR_a \approx 11dB$; (b) image obtained with the laser controlled by the electronic feedback loop (i.e. $\tau_R \approx 3\mu s$) and giving $SNR_b \approx 17\,dB$. Experimental conditions: $P_{out} \approx 10\,mW$ (i.e. $p_{out} \approx 5\times10^{16}\ photons/s$ at $\lambda = 1064\,nm$), $\mathrm{F_R} \approx 950\,\mathrm{kHz}$; $F_e \approx 1.05\times F_R$; $R_{bs} = 0.5$ and $T_{\mathrm{int}} = 50\mu s$. The SNR have been calculated by dividing the mean values of the measured signals on the ruler (right rectangle) and outside the ruler (left rectangle). The effective reflectivity of the ruler is estimated to be : $\langle \mathrm{R_e} \rangle \approx 2\times10^{-10}$, which corresponds to the detection of: $\mathrm{R_e}\times(1-\mathrm{R_{bs}})^2\times \mathrm{p_{out}}\times 50\,\mu\mathrm{s} \approx 160\,\mathrm{photons}$ for each pixel of the bright part of the ruler.

Table 1. LOFI SNR for the free running laser (i.e. $\tau_R \approx 50\mu s$); and for the laser with the electronic feedback control (i.e. $\tau_R \approx 3\mu s$); The laser is a class-B laser with: $p_{out} \approx 5\times10^{16}\ photons/s$ ($P_{out} \approx 10mW$ at $\lambda = 1064\,\mathrm{nm}$) and $\mathrm{F_R} \approx 950\,\mathrm{kHz}$. The experimental conditions are: $F_e \approx 1.05\times F_R$, $\mathrm{R_{bs}} = 0.5$, and $R_e \approx 4\times10^{-10}$.

T_{int}:	5 μs	10 μs	20 μs	50 μs
Numerical simulations: (Fig. 4)				
$\mathrm{SNR_{LOFI}}$ for $\tau_R \approx 50\mu s$	2	2	5.1	7.8
$\mathrm{SNR_{LOFI}}$ for $\tau_R \approx 3\mu s$	3.5	4.1	7.1	9.2
Experimental results: (Fig. 4)				
$\mathrm{SNR_{LOFI}}$ for $\tau_R \approx 50\mu s$	2.5	2.6	7.1	7.2
$\mathrm{SNR_{LOFI}}$ for $\tau_R \approx 3\mu s$	4.3	5.6	7.2	22.3
Analytical expression: [Eq. (24)]				
$\mathrm{SNR_{LOFI}}$ for $\tau_R \approx 50\mu s$	2.4	3.1	4.5	8.6
$\mathrm{SNR_{LOFI}}$ for $\tau_R \approx 3\mu s$	4.5	5.1	7.8	11.8
LOFI shot-noise limit : [Eq. (25)]				
$\mathrm{SNR_{SN}}$	3.5	5.0	7.0	11.1